Eur. Phys. J. D (2016) 70: 100
DOI: 10.1140/epjd/e2016-70085-9

THE EUROPEAN PHYSICAL JOURNAL D

Regular Article

Change in resonance parameters of a linear molecule as it bends: Evidence in electron-impact vibrational transitions of hot COS and CO_2 molecules*

Masamitsu Hoshino[1,a], Yohei Ishijima[1], Hidetoshi Kato[1], Daisuke Mogi[2], Yoshinao Takahashi[3], Katsuya Fukae[4], Paulo Limão-Vieira[5], Hiroshi Tanaka[1], and Isao Shimamura[6]

[1] Department of Physics, Sophia University, Chiyoda-ku, 102-8554 Tokyo, Japan
[2] Fine Chemicals Sales Dept.-III, Sales Div., Kanto Denka Kogyo Co., Ltd., Chiyoda-ku, 101-0063 Tokyo, Japan
[3] Development & Marketing Management Dept., New Products Development Div., Kanto Denka Kogyo Co., Ltd., Chiyoda-ku, 101-0063 Tokyo, Japan
[4] Shibukawa Decelopment Research Lab., New Products Development Div., Kanto Denka Kogyo Co., Ltd., Shibukawa-shi, 377-0008 Gunma, Japan
[5] Laboratório de Colisões Atómicas e Moleculares, CEFITEC, Departamento de Física, Faculdade de Ciências e Tecnologia, Universidade Nova de Lisboa, 2829-516 Caparica, Portugal
[6] Atomic Physics Research Unit, RIKEN, Hirosawa 2-1, Wako, 351-0198 Saitama, Japan

Received 8 February 2016 / Received in final form 14 March 2016
Published online 3 May 2016 –

Abstract. Inelastic and superelastic electron-impact vibrational excitation functions of hot carbonyl sulphide COS (and hot CO_2) are measured for electron energies from 0.5 to 3.0 eV (1.5 to 6.0 eV) and at a scattering angle of 90°. Based on the vibrational populations and the principle of detailed balance, these excitation functions are decomposed into contributions from state-to-state vibrational transitions involving up to the second bending overtone (030) in the electronically ground state. Both the $^2\Pi$ resonance for COS around 1.2 eV and the $^2\Pi_u$ resonance for CO_2 around 3.8 eV are shifted to lower energies as the initial vibrational state is excited in the bending mode. The width of the resonance hump for COS changes only little as the molecule bends, whereas that of the overall boomerang resonance for CO_2 becomes narrower. The angular distribution of the electrons resonantly scattered by hot COS and hot CO_2 is also measured. The different shapes depending on the vibrational transitions and gas temperatures are discussed in terms of the symmetry of the vibrational wave functions.

1 Introduction

Atomic resonances are controllable by external fields. Indeed, the effects of a static electric field on resonances in photoionization and photodetachment have been studied extensively [1–3]. Moreover, magnetic fields have been widely used to shift extremely low-energy Feshbach resonances to control properties of Bose-Einstein condensates and other ultracold degenerate quantum gases such as fermion gases and boson-fermion mixtures [4,5].

Properties of molecular resonances depend on the nuclear configuration and can be controlled by vibrational excitation, which influences not only the resonance position and the width but even the symmetry property of the resonance state. Thus, Rescigno et al. [6] and McCurdy et al. [7] studied in detail the splitting of a doubly degenerate $^2\Pi_u$ resonance state of linear CO_2^- at ∼3.8 eV into two nondegenerate Renner-Teller states [8] of symmetry $^2A_1$ and $^2B_1$ as the molecular ion bends. Based on the knowledge of the complex potential energy surfaces (CPES) as functions of the nuclear configuration these authors calculated the vibrational excitation cross sections using a generalized version of the boomerang model to elucidate the role of the CPES in the dynamics of the relevant resonance processes. An earlier work by Hopper et al. [9] deals with a similar $^2\Pi$ resonance in the asymmetric linear molecule N_2O^-, showing the split into nondegenerate resonances of symmetry $^2A'$ and $^2A''$ upon bending.

The bending motion is controllable by raising the vibrational temperature of the initial target molecules in electron impact experiments. Therefore, employing such a technique through an extensive set of measurements using hot molecular gas beams is of particular importance in elucidating the symmetry and nuclear-configuration dependent dynamics of molecular resonance processes. Indeed, we succeeded in observing the lowering of the $^2\Pi_u$

* Contribution to the Topical Issue "Advances in Positron and Electron Scattering", edited by Paulo Limao-Vieira, Gustavo Garcia, E. Krishnakumar, James Sullivan, Hajime Tanuma and Zoran Petrovic.

[a] e-mail: masami-h@sophia.ac.jp

resonance in electron-impact vibrational excitation of CO_2 at ∼3.8 eV, as the vibrational temperature increases [10]. We also observed a similar phenomenon for the $^2\Pi$ resonance in vibrational excitation of N_2O at ∼2.3 eV [11]. The present work extends this investigation to electron scattering by carbonyl sulphide COS, a linear asymmetric molecule S=C=O in equilibrium in the vibronically ground state.

Vibrational excitation of COS by low-energy electron impact is characterized by a few prominent features. In particular, extensive experimental studies have been focused on the cross section enhancement at 1.2–1.3 eV by Szmytkowski and Zubek [12], by Tronc and Azria [13], by Sohn et al. [14], by Abouaf et al. [15], and in more detail by Hoffmann et al. [16]. This cross section enhancement is due to a $^2\Pi$ shape resonance as has been found by Lynch et al. [17] in their elastic scattering calculation using the continuum multiple scattering model with a local exchange potential. This resonance has been confirmed later by more sophisticated calculations of Michelin et al. [18], Bettega et al. [19], and Gianturco and Stoecklin [20]. Another, broad feature, found around 3.7 eV, is assigned to the overlapping of $^2\Sigma$ and $^2\Delta$ resonances [14].

The $^2\Sigma$ component of the cross section shows a narrow peak close to the vibrational threshold [14–16], which stems from a virtual state [19] and occurs also in elastic scattering in the low-energy limit. As the impact energy increases, this peak in the $^2\Sigma$ elastic integral cross section (ICS) decays gradually, and a shallow Ramsauer-Townsend minimum follows at ∼0.6 eV [20] (or at ∼1.0 eV according to Ref. [21]). This theoretical minimum in the $^2\Sigma$ ICS, however, is not really measurable because of the addition of a much larger $^2\Pi$ ICS, which shows a more pronounced minimum [19,20]. The minimum in the measured total ICS is mainly due to the $^2\Pi$ ICS; see discussion in Section 3.1 for further detail. Similar minimum has been observed in the energy dependence of the elastic differential cross section (DCS) at large scattering angles [14,16].

For absolute measurement of the elastic DCS in a wide energy region, see reference [22] and references therein. Reviews of the various processes occurring in electron collisions with COS can be found in references [16,22,23]

From the quantum chemical point of view, CO_2, COS, and CS_2 are closely related triatomic linear molecules in the electronically ground state. The spherical part of their polarizability ranges from 19.6 a.u. (CO_2) via 38.5 a.u. (COS) to 59.8 a.u. (CS_2) [24]. Only COS, being asymmetric, has a permanent dipole moment of 0.715 D [25]. Table 1 summarizes some molecular constants of COS, including the isotropic and anisotropic polarizabilities [26] and the vibrational quanta of the fundamental modes [27].

The COS molecule has been of particular interest because of its importance in the global cycling of sulfur and as a source of biogenic sulfur [28–32]. It has been observed in the interstellar medium and in the upper atmospheres of Venus and Jupiter [33–36]. Furthermore, COS is used technologically as a new additive gas for fine plasma etching of semiconductors [37].

Table 1. Molecular constants of COS in the electronically ground state.

Bond distance (Å)	C–O	1.16[a]
	C–S	1.56[a]
Bond angle (°)		180
Symmetry		$C_{\infty v}$
Dipole moment (D)		0.715[b]
Polarizability (Å^3)	α_0: isotropic	5.21[c]
	α_2: anisotropic	4.02[c]
Vibrational mode	Quantum (eV)[d]	Symmetry
ν_1 mainly CS stretching	0.107	σ
ν_2 Bending	0.065	π
ν_3 mainly CO stretching	0.254	σ

[a]Reference [24], [b]reference [25], [c]reference [26], [d]reference [27].

We note a general recognition in regard to the urgent need for comprehensive studies and detailed knowledge of low-energy electron collisions with vibrationally and rotationally (and even electronically) excited molecules for modeling the behavior of gas discharges, plasmas, gaseous dielectrics and pulse power switches [38]. Conventionally, however, electron collisions with COS molecules have been measured only for the target gas at room temperature. Likewise, calculations of vibrational excitation have been limited to the vibrationally ground state as the initial state. The paucity of experimental data for "hot" molecules stems mainly from the difficulty in producing a sufficient number of excited species for collision experiments under well-controlled conditions. The few measurements for vibrationally excited molecules found in the literature have employed heating sources, laser photons or monoenergetic electrons to excite the molecules vibrationally.

At Sophia University, we are developing a comprehensive program for unraveling dynamic processes involving hot molecules. We have reported the results for electron scattering by hot CO_2 [10] and by hot N_2O [11]. This project originates from our studies on the total ion yields by inner-shell ionization of hot CO_2 [39], hot N_2O [40], and hot CF_3I [41] probed by the synchrotron radiation source Spring-8, RIKEN, Japan and from the photoabsorption spectroscopy of the hot CO_2 and hot COS molecules [42] at the Photon Factory, KEK, Japan. In the present work electron energy-loss spectra of hot COS are measured in the energy region from 0.5 to 3 eV including the $^2\Pi$ resonance. Based on the known vibrational populations and the principle of detailed balance, the intensities of the inelastic and superelastic peaks in the energy-loss spectra are decomposed into the contributions from different vibrational transitions according to the technique discussed in reference [11] and applied to hot N_2O. Furthermore, our previously measured energy-loss spectra for hot CO_2 [10] were reanalyzed with this technique.

The next section briefly describes our experimental arrangement, measurement procedure and the analysis techniques. Section 3 is devoted to the presentation of our results followed by some discussion. Finally, Section 4 concludes this work.

2 Experimental and analysis

2.1 Apparatus and data-unfolding procedures

Detailed description of the electron spectrometer is found in references [43,44]. Briefly, an electron beam from an electrostatic hemispherical monochromator crosses an effusive molecular beam of hot COS molecules at right angles. Scattered electrons are energy analyzed by a second electrostatic hemispherical system. The whole electron spectrometer is enclosed in separate casings and pumped differentially to reduce variation of the electron beam current with different gases. The overall energy resolution is ∼30 meV and the incident current is 0.5–1.5 nA for the incident electron energy from 0.5 to 3.0 eV. The entire electron optics has been designed by beam tracing methods. They use computer-controlled voltages which follow the energy sweeps, for maintaining constant transmission and beam focus conditions. The relative flow method [45] is used to put the measured data on an absolute scale using the absolute helium cross section given in reference [46] corrected for the effect of the target gas temperature T and pressure P on the gas flux $J \propto P/\sqrt{T}$. The energy scale of the incident electrons is calibrated against a He^- Feshbach resonance at 19.366 eV [47], as well as the first peak at 1.980 eV in a $^2\Pi_g$ resonance region in the cross section for electron impact vibrational excitation $v = 0 \rightarrow 1$ of N_2 [48]. We expect this calibration to be accurate within ±10 meV.

The resistive method for heating the molecular gas has been described elsewhere [10,11]. A cylindrical cell made of solid copper (Cu), incorporating a 4 mm-long nozzle of 0.6 mm and 0.3 mm outer and inner diameters, is used. The cell has an internal deameter of 10 mm and a length of 12 mm, fitted with a quartz fiber. The cell is heated by wrapping a resistive coaxial sheath wire around it. A calibrated thermocouple is set in a small hole on the cell and monitors the cell temperature, which reaches even above ∼800 K. A magnetic shield around the cell prevents the field generated by the heater (around which is wrapped a water flowing pipe that can cool as an outer jacket) from penetrating into the interaction region.

The scattering spectrometer can be operated in two modes. First, measurements of the angular dependence of any discrete excitation process are performed by studying the intensity $I(\Delta E; E)$ of the scattered electron signal at one specific energy loss ΔE for a fixed impact energy E. Figure 1 shows examples of the electron energy-loss spectrum for COS at two different temperatures 300 and 730 K at a scattering angle of 90° and $E = 1.2$ eV in the region of the $^2\Pi$ resonance. Peak 1 on the left side of the elastic peak represents energy gain or a superelastic process, whereas peaks on the right side represent energy loss or excitation processes. All the peaks in Figure 1 are ascribed mainly to the contributions from the bending mode.

With the present energy resolution of ∼30 meV the tail on the left of the elastic peak overlaps the superelastic peak and that on the right the first excitation peak. It may be noticed that a single spherical analyzer with virtual slits allows some electrons with energies off the mean pass energy in the sphere (∼1.5 eV) to pass by reflection from the walls, which form intrinsically a longer tail on the loss side of the elastic peak. The elastic peak for the helium target together with this background can reproduce that long tail fairly well. We therefore use it to subtract the background, which is inherent in the present measurements. Then, the difficulty with the peak overlap is partially resolved and the Gaussian-profile fitting reproduces well the features of the observed spectrum.

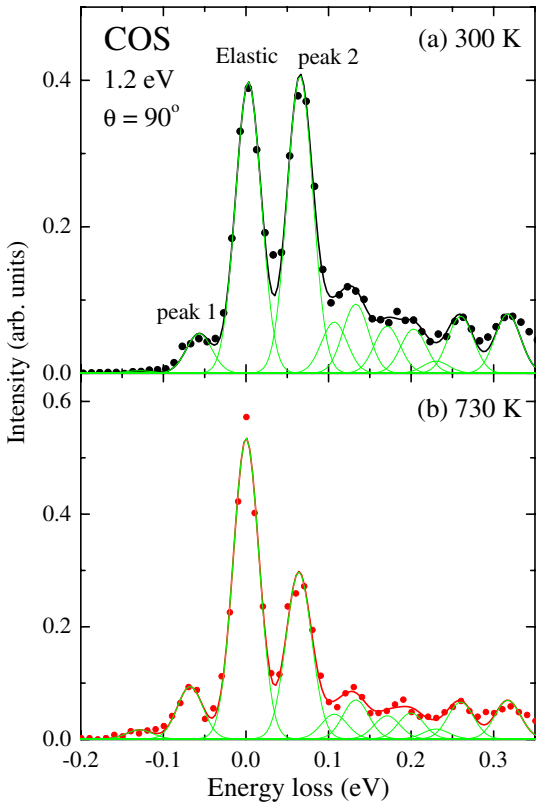

Fig. 1. Typical electron energy-loss spectra for COS recorded at temperatures 300 and 730 K at a scattering angle of 90° and $E = 1.2$ eV in the region of the $^2\Pi$ resonance.

For studying the resonance profile, the analyzer is tuned to transmit only the electrons corresponding to specific energy-loss channels ($\Delta E = -0.065$ eV, 0 eV, and 0.065 eV) and the count rate measured as a function of the impact energy E. In the present measurements of vibrational excitation, the background originating from the tail of the elastic peak is assumed to have the same energy dependence as the elastic peak, which is subtracted from the vibrational spectra.

For vibrational transitions in resonant electron scattering by a molecule M, the ratio of the lifetime τ_r of the temporarily formed compound ion M^- to the vibrational period τ_ν affects decisively the shape of the E-dependent cross sections [49]. Thus, Herzenberg and Mandl [50] noted that, for $\tau_r \gg \tau_\nu$, or in the compound-molecule limit, the ion M^- has enough time for developing vibrational states, which manifest themselves in the cross section as equally spaced, regular peaks occurring at common positions for any vibrational transition. For $\tau_r \ll \tau_\nu$, or in the impulse

limit, the ion M^- has hardly any time for nuclear motion before it decays; the impulse (or adiabatic) approximation for the vibrational motion applies to this case. Thus, the scattering amplitude is a superposition of resonance scattering amplitudes with a nuclear-configuration-dependent resonance position and width, producing a structureless, broad hump in the cross section.

For the intermediate case, $\tau_r \simeq \tau_\nu$, the ion M^- has insufficient time for forming well-defined vibrational states, but the wave packet for the vibrational motion makes one or a few complete oscillations before the ion decays. A theoretical description based on a single-oscillation picture, called the boomerang model, was developed by Herzenberg [51,52]. Its applications to the $^2\Pi_g$ resonance in electron scattering by N_2 at 2∼3 eV, and later to some other molecular resonances with $\tau_r \simeq \tau_\nu$, have successfully reproduced the typically irregular resonance structures with peaks unequally spaced and shifted depending on the particular vibrational transition. These structures are sometimes referred to as vibrational structures in the literature, in spite of the fact that those peaks are clearly unassociated with any well-defined vibrational levels of the resonance state.

The broad $^2\Pi$ resonance for electron scattering by COS at ∼1.2 eV with no fine structure [13–19,22] is evidently an impulse-limit resonance. We assume that the impulse approximation can be simplified into the fixed-nuclei approximation without too much error. Then, the shape of the cross section for each particular vibrational transition may be represented by a Breit-Wigner one-level formula. We note that the measured excitation functions for COS are superpositions of the cross sections for different vibrational transitions corresponding to slightly different nuclear configurations, and hence, having slightly different resonance positions and widths (see Sect. 2.2, Eqs. (1)). However, considering the limited experimental energy resolution and the statistical error stemming from the time-consuming measurements with the temperature control, we expect that each of the present measured excitation functions may be safely smoothed by a Breit-Wigner fit after subtraction of the tail contribution from the elastic peak.

For the $^2\Pi_u$ resonance in scattering by CO_2 at ∼3.8 eV the lifetime τ_r is known to be comparable to the vibrational period τ_ν, and a clear fine structure, explainable by the boomerang model, appears in the vibrational cross sections [53–57]. In our present measurement at high temperatures, however, the statistical error prevents the fine structure from being observed accurately enough. Our compromise is to fit some analytical function without a fine structure to the measured data for the purpose of smoothing. For this purpose we have chosen for convenience the Breit-Wigner formula with a background linear in E.

2.2 Determination of the state-to-state cross sections

A vibrational state of the asymmetric molecule COS is denoted by the quantum numbers $(\nu_1 \nu_2^l \nu_3)$ (see Tab. 1) with ν_1 for the normal mode of mainly CS stretching (similar to the symmetric stretching of a symmetric molecule such as CO_2), ν_3 for the normal mode of mainly CO stretching (similar to the asymmetric stretching of CO_2), ν_2 for the bending vibration and l for the vibrational angular momentum, which is omitted when all values of l for that ν_2 are collectively denoted, or often omitted when only one value of l is allowed for that ν_2.

Table 2. The excitation energies, degeneracies g_ν, and the population fractions $P(T)$ at temperature T (K) of some lowest vibrational states of COS in the ground electronic state, and their grouping into nearly degenerate states.

Group No.	State $(\nu_1 \nu_2^l \nu_3)$	Energy[a] (eV)	g_ν	Population fractions $P(300)$	$P(530)$	$P(730)$
0	(00^00)	0.000	1	0.8310	0.5322	0.3680
1	(01^10)	0.065	2	0.1371	0.2593	0.2633
2	(10^00)	0.107	1	0.0134	0.0515	0.0673
	(02^00)	0.129	1	0.0057	0.0316	0.0472
	(02^20)	0.137	2	0.0083	0.0529	0.0831
3	(11^10)	0.171	2	0.0022	0.0250	0.0481
	(03^10)	0.193	2	0.0009	0.0154	0.0339
	(03^30)	0.193	2	0.0009	0.0155	0.0341
	(20^00)	0.213	1	0.0002	0.0051	0.0125

[a]Reference [27].

For practical definition of "state-to-state" DCS, we treat unresolvable near-degenerate or closely spaced vibrational states as a whole. In other words, we classify the vibrational states into groups as specified in Table 2. Thus, we refer to the transition from group 1 to group 2 in the sense of that from (010) to any of (100), (02^00), and (02^20), the associated DCS being denoted by σ_{12}. For CO_2, Fermi resonance coupling occurs between the symmetric stretching and bending modes, for example, a dyad formed from the states (100) and (02^00) [56,57]. With our present resolution and statistical error this dyad is measured as a whole together with the nearby state (02^20) unresolved. The exception is the angular distribution data reported in Section 3.3. There, the energy-loss peak for the Fermi dyad is carefully decomposed into its two members. Similarly, the peaks for group 2 are decomposed into the members (100) and (020).

The "group-to-group" DCS σ_{AB} depends, in principle, on the temperature T. It is independent of T if the initial-state group A has only one member or if all of its members can be regarded as degenerate [11]. The T-independence is assumed in the following argument.

A previous publication [11] details the procedure for extracting the group-to-group DCS σ_{AB} from the intensities of the superelastic (such as peak 1 in Fig. 1) and of the first excitation peak (such as peak 2 in the same figure). The peak intensities, transformed into the dimension of the cross sections, are expressible as:

$$\sigma_{\rm sup}(E,T) = P_1(T)\sigma_{10}(E) + P_2(T)\sigma_{21}(E) + P_3(T)\sigma_{32}(E)$$
$$\sigma_{\rm exc}(E,T) = P_0(T)\sigma_{01}(E) + P_1(T)\sigma_{12}(E) + P_2(T)\sigma_{23}(E) \quad (1)$$

in terms of the partial populations $P_A(T)$ of groups A (see Tab. 2) calculated from the Boltzmann distribution at temperature T, to the extent that the partial populations for further terms on the right-hand sides are negligibly small.

Similarly, the elastic peak is expressible as:

$$\sigma_{\rm elas}(E,T) = P_0(T)\sigma_{00}(E) + P_1(T)\sigma_{11}(E) + P_2(T)\sigma_{22}(E) \quad (2)$$

if further terms are negligible.

The three cross sections $\sigma_{ii}(E)$, treated as unknown parameters in equation (2), may be determined if the elastic peak is measured at three or more different temperatures. For the analysis of the excitation and superelastic peaks, further simplification applies as is described below.

The principle of detailed balance, which relates a process to its reverse process, follows from the quantum mechanical time-reversal symmetry [58]. This general and rigorous principle leads, in turn, to a relation

$$E_A g_A \sigma_{AB}(E_A) = E_B g_B \sigma_{BA}(E_B) \quad (3)$$

between the state-to-state cross section for a transition from group A to group B (with an excitation energy ΔE) at a collision energy $E = E_A$ and that for the reverse process at $E = E_B = E_A - \Delta E$, provided that all the members of each group be degenerate [11], which is the case with the present problem approximately; g_A and g_B are the degeneracies of the groups found from Table 2.

For application of this relation to the analysis of the energy-loss spectra, for which the collision energy E is common for both the superelastic and excitation peaks, a further approximation $\sigma_{AB}(E_A) \simeq \sigma_{AB}(E_B)$, or $\sigma_{BA}(E_B) \simeq \sigma_{BA}(E_A)$ is necessary. This approximation is invalid when the cross section varies rapidly with E between E_A and E_B, as may be the case with (i) the near-threshold energy region; (ii) especially, a threshold peak due to a weakly bound or virtual state, and with (iii) low-energy, forward scattering by polar molecules governed by the long-range dipole potential. In principle, the finite experimental energy resolution may also complicate the analysis. When the above approximation appears to be valid within the experimental uncertainty, equation (3) reduces, in the present case, to

$$\begin{aligned} 1 \times E\sigma_{01} &= 2 \times (E - \Delta E_{01})\sigma_{10}, \\ 2 \times E\sigma_{12} &= 4 \times (E - \Delta E_{12})\sigma_{21}, \\ 4 \times E\sigma_{23} &= 6 \times (E - \Delta E_{23})\sigma_{32}. \end{aligned} \quad (4)$$

The measured peak intensities in the energy-loss spectra, or the cross sections $\sigma_{\rm sup}(E,T)$ and $\sigma_{\rm exc}(E,T)$, may be analyzed by treating the state-to-state cross sections σ_{AB} in equations (1) as unknown parameters to be determined by coupling all the equations for different temperatures T; $T = 300, 530$, and 730 K in the present case for COS, and $T = 300, 520$, and 830 K for CO_2. Further incorporation of equation (4) reduces the number of unknown parameters from six to only three, which should be small enough for a reliable determination of the DCS σ_{AB}.

3 Results and discussion

3.1 "Effective" excitation functions measured at different temperatures

Figure 2 shows examples of the measured excitation functions, in the form of the absolute DCSs, for vibrationally elastic ($\Delta E = 0$ eV), superelastic ($\Delta E = -0.065$ eV), and inelastic ($\Delta E = 0.065$ eV) scattering of electrons from COS in the ground electronic state observed at temperatures T of 300 K, 530 K, and 730 K. The data available in the literature for comparison are at room temperature only. The present results for $T = 300$ K are in excellent agreement with those from Sohn et al. [14], Abouaf et al. [15], and Hoffmann et al. [16], and with the previous absolute cross sections determined above 2 eV [22].

Figure 2b clearly reveals the change in the position of the resonance maximum and the apparent width as the gas temperature increases, indicating qualitatively the effects of the bending excitation, or the change in the molecular geometry. The resonance profiles of the state-to-state vibrational cross sections will be presented in the next section.

Note that the measured, T-dependent DCSs $\sigma_{\rm sup}(E,T)$ and $\sigma_{\rm exc}(E,T)$ in equations (1) do not directly represent the collision dynamics. They are merely apparent or effective cross sections in the form of T-dependent linear combinations of the physical cross sections for different vibrational transitions with different energy and angular distributions.

For example, all coefficients $P_A(T)$ in $\sigma_{\rm sup}(E,T)$ in equations (1) are small for low temperatures, $P_0(T)$ being close to unity, then. Therefore, the values of $\sigma_{\rm sup}(E,T)$ will be small for low T. These small $\sigma_{\rm sup}(E,T)$ do not necessarily suggest small superelastic cross sections σ_{10}, σ_{21}, and σ_{32}. The small effective cross sections $\sigma_{\rm sup}(E,T)$ for low T are due merely to the fact that most molecules are in the ground state and never lose their internal energy. Even at room temperature, the superelastic excitation function in Figure 2b is much smaller than the inelastic excitation function.

The superelastic effective cross section $\sigma_{\rm sup}(E,T)$ can sometimes be strongly affected by the rise in the temperature. Since it contains no contributions from the ground state (000), the change in the excited-state population $1 - P_0(T)$ with T directly influences $\sigma_{\rm sup}(E,T)$. Indeed, in Section 3.3, we will see a remarkable example of the increase in the value of $1 - P_0(T)$ for CO_2 by a factor of more than five when going from 310 to 720 K, which is reflected in the considerable enhancement of $\sigma_{\rm sup}(E,T)$.

The energy or angular distribution of $\sigma_{\rm sup}(E,T)$ or $\sigma_{\rm exc}(E,T)$ is the result of a T-dependent linear combination of three different energy or angular distributions σ_{10}, σ_{21}, and σ_{32} or σ_{01}, σ_{12}, and σ_{23}. Thus, for example, even when the resonance profiles of $\sigma_{01}(E)$, $\sigma_{12}(E)$, and $\sigma_{23}(E)$ are nearly Lorentzian, the effective cross section $\sigma_{\rm exc}(E,T)$ will have a profile different from a single Lorentzian, if the three vibrational transitions have different resonance positions and widths.

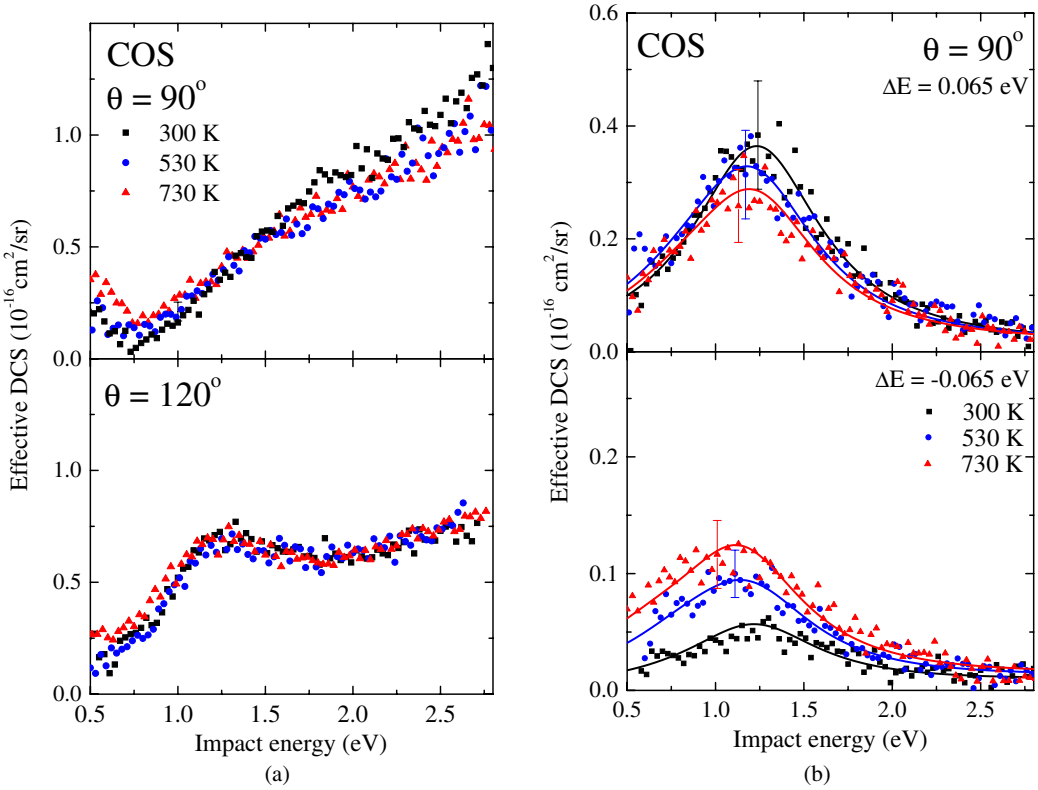

Fig. 2. Measured excitation functions, put on the scale of the absolute differential cross sections, for (a) vibrationally elastic ($\Delta E = 0$ eV) and (b) superelastic ($\Delta E = -0.065$ eV) and inelastic ($\Delta E = 0.065$ eV) scattering of electrons from COS at temperatures of 300, 530, and 730 K. They are "effective" cross sections in the sence of mere linear combinations, equations (1), of the physical cross sections for a few vibrational transitions, the coefficients varying with the temperature.

In a similar way, the effective elastic cross section, equation (2), may exhibit quite different size and angular or energy distribution depending on the temperature if $\sigma_{00}(E)$, $\sigma_{11}(E)$, and $\sigma_{22}(E)$ are quite different from each other.

Note also that no simple relation between $\sigma_{\rm sup}(E,T)$ and $\sigma_{\rm exc}(E,T)$, such as equation (4), follows from the principle of detailed balance. Thus, these two effective cross sections have, in general, different angular and energy distributions.

In a hot molecular gas rotational states are also excited more than in a cold gas. That might increase dissociative attachment cross sections, though less conspicuously than for high vibrational temperatures [59–62]. The elastic and vibrational excitation cross sections we measure, however, are unaffected by the rotational temperature. This is because the collision time is much shorter than the typical rotational period in the present collision condition (except for extremely forward scattering governed by extremely distant collisions), and hence, the adiabatic-rotation approximation is valid. In this approximation, the cross section summed over the final rotational states (which we measure with the present energy resolution) is proved to be independent of the initial rotational state, or of the initial rotational temperature [63,64].

The minimum in the elastic DCS, such as seen in Figure 2a around 0.7 eV, has been known for some time [14,16], and has been associated with the Ramsauer-Townsend (RT) effect [16]. In fact, this interpretation is questionable. In theoretical calculations in the fixed-nuclei approximation, the $^2\Sigma$ eigenphase sum has been found to decrease with energy and to turn from positive to negative values across zero in the energy region 0.6–1.0 eV. This introduces a shallow RT minimum in the $^2\Sigma$ component of the elastic integral cross section (ICS) dominated by s-wave scattering [20,21]. However, the $^2\Pi$ contribution is much larger around the $^2\Sigma$ RT minimum. As a result, the total elastic ICS exhibits a pronounced minimum originating from the combination of the left-hand tail of the $^2\Pi$ resonance peak and the increase of the ICS toward low energies due to the $^2\Sigma$ virtual state and to the effect of the long-range dipole interaction [19,20].

The energy dependence of the elastic DCSs at fixed scattering angles θ is not reported in the theoretical papers [19,20]. Though a definite conclusion is difficult to draw, the main origin of the pronounced minimum in Figure 2a for $\theta = 120°$ and in the experimental DCSs for $\theta = 130°$ and 135° reported in references [14,16] is most probably the combination of the tail of the $^2\Pi$ resonance and the virtual-state rise toward low energies, with the dipole potential contribution being unimportant in scattering by large angles. The data for $\theta = 90°$ in Figure 2a without the $^2\Pi$ resonance peak are exceptional since the angular distribution of elastic scattering in the region of

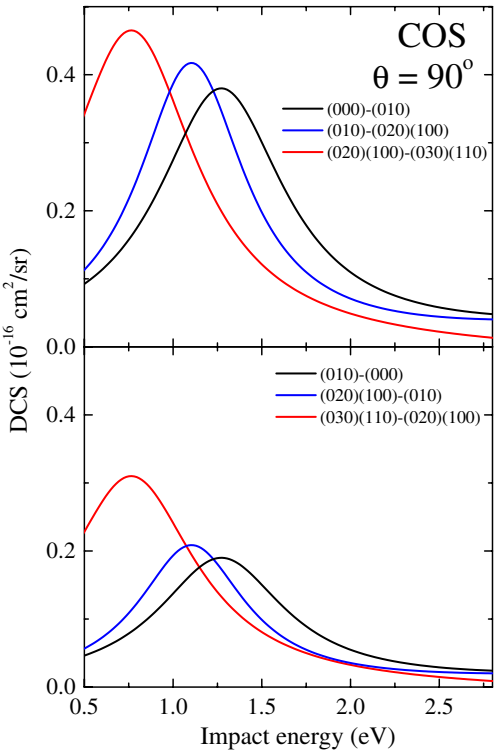

Fig. 3. The absolute state-to-state excitation functions for $^2\Pi$ resonance scattering of electrons by COS at $\theta = 90°$ extracted by using equations (1) and the principle of detailed balance (4).

this resonance drops sharply near $\theta = 90°$ (Sect. 3.3); the DCS on the right of the minimum keeps rising beyond the energy region of the $^2\Pi$ resonance.

Although the position and the depth of the minimum are difficult to determine accurately with our present energy resolution and the statistical error, the minimum appears to shift slightly toward higher energies and to become shallower with the increase of the vibrational temperature in the bending mode.

3.2 State-to-state vibrational cross sections

Figure 3 shows the absolute state-to-state excitation functions for the $^2\Pi$ resonance scattering by COS at $\theta = 90°$ extracted from the data in Figure 2b by using equations (1) and the principle of detailed balance (4).

For comparison Figure 4b shows similar state-to-state excitation functions for the $^2\Pi_u$ resonance scattering by CO_2, obtained by reanalysis of the previously measured data shown in Figure 4a [10]. With the present energy resolution the boomerang fine structure is observed in the effective excitation function at room temperature only, where the signal-to-noise ratio is much better than at high temperatures. The lack of the fine-structure information at high temperatures forces the extraction of the state-to-state cross sections to be based on the average, broad resonance peaks in the effective cross sections.

The detailed balance relation (4) is seen to be satisfied by the results shown in Figures 3 and 4, unlike those in reference [10]. Incidentally, the superelastic excitation function is much smaller than the inelastic one, which has already been explained in the previous subsection in regard to Figure 2b.

For both COS and CO_2 the resonance profile is shifted to lower energies as the initial vibrational level is excited as σ_{01}, σ_{12}, and σ_{23}, i.e., as the molecule bends, though the bent state (020) is mixed with the stretched state (100), and (030) with (110). This resonance lowering trend is also found for the $^2\Pi$ resonance in vibrational excitation of N_2O at ∼2.3 eV [11]. The $^2\Pi$ resonance in question is of the impulse-limit type for both of the asymmetric linear molecules COS and N_2O. Therefore, the knowledge of the complex potential energy surfaces of the resonance states of COS^- or N_2O^- is of direct use in interpreting the state-to-state cross sections. Thus, we note in reference [11] that the $^2\Pi$ resonance of the linear N_2O^- splits into nondegenerate levels of symmetry $^2A'$ and $^2A''$ upon bending, of which the lower-lying $^2A'$ state plays a more important role since it shifts to lower and lower energies by bending [9] in consistency with the trend in the state-to-state cross sections. Unfortunately, we are unaware of any resonance calculations for bent COS^-, and can only infer by close comparison with N_2O^-.

Since the $^2\Pi_u$ resonance in electron scattering by CO_2 is of the boomerang type, the resonance profile is difficult to deduce directly from the knowledge of the fixed-nuclei resonances of CO_2^-. Only after nuclear dynamics calculations, such as in references [6,7], can one discuss this resonance in detail. In those calculations not only the Renner-Teller splitting of the $^2\Pi_u$ resonance into the symmetry $^2A_1$ and $^2B_1$ but also the Fermi coupling of the CO_2 vibrational modes introduces further complexity as is detailed in reference [7]. In particular, the boomerang model developed by Herzenberg [51,52] must be generalized for multidimensional nuclear motion for dealing with polyatomic molecules. Furthermore, it was found that the $^2A_1$ complex potential surface alone is incapable of reproducing the boomerang fine structure [6]. The structure appears only after nonadiabatically coupling the $^2A_1$ surface with the $^2B_1$ surface [7].

Table 3 summarizes the effect of the change in the initial vibrational state on the maximum position and the apparent width of the whole resonance profile for COS and CO_2. The width of the impulse-limit resonance in the asymmetric molecule COS or N_2O is only weakly affected by this change, whereas the overall width of the boomerang resonance in the symmetric molecule CO_2 decreases markedly.

The magnitude of the resonance cross sections for COS (Fig. 3) and N_2O (Ref. [11]) increases as the initial state bends. On the contrary, that for CO_2 decreases as it bends (Fig. 4). Naturally, the same trend is observed for vibrational deexcitation because of the principle of detailed balance.

Incidentally, Ferch et al. [65] measured the effective total cross section for electron-CO_2 scattering in a transmission experiment at $T = 250$ and 520 K, from which they extracted the total cross sections for CO_2 in the

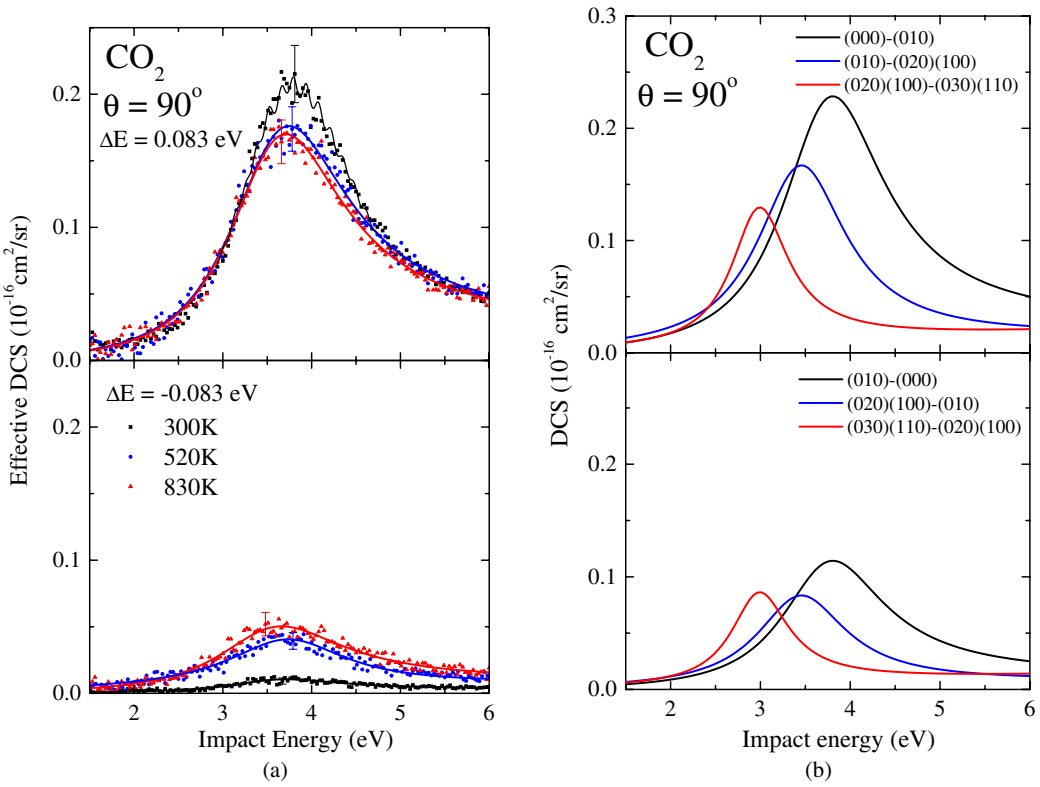

Fig. 4. (a) Measured excitation functions, put on the scale of the absolute differential cross sections, for superelastic ($\Delta E = -0.083$ eV) and inelastic ($\Delta E = 0.083$ eV) scattering of electrons from CO_2 for a scattering angle of 90° and at temperatures of 300, 520, and 830 K. (b) The absolute state-to-state excitation functions for the $^2\Pi_u$ resonance scattering by CO_2 around 3.4 eV, obtained by reanalysis of the data from reference [10] based on equations (1) and the principle of detailed balance (4).

Table 3. The maximum position (E_{max}) and the full width at half maximum (FWHM) of the $^2\Pi$ resonance profile in the differential cross section for state-to-state vibrational excitation at $\theta = 90°$.

Transition	COS (E_{max}, FWHM) eV	CO_2 (E_{max}, FWHM) eV
(000)–(010)	(∼1.3, ∼0.9)	(∼3.8, ∼1.5)
(010)–(020)(100)	(∼1.1, ∼0.8)	(∼3.4, ∼1.3)
(020)(100)–(030)(110)	(∼0.8, ∼0.9)	(∼3.0, ∼0.8)

ground vibrational state (σ_0) and in excited vibrational states (σ_{exc}). In this extraction procedure they assumed σ_{exc} to be independent of the initial vibrational state. Although this approximation may not hold accurately, one may get a rough idea of the effect of the initial bending on the total cross sections. The $^2\Pi_u$ resonance maximum in σ_{exc} occurs at about 0.3 eV lower than in σ_0 and the peak in σ_{exc} is higher than σ_0 by about 35% and broader by about 8%. Our results on the state-to-state DCS at $\theta = 90°$ cannot be compared directly with these total cross sections with a strong influence of the dipole interaction. Nevertheless, the resonance lowering by bending appears to be consistent with our results.

3.3 Angular distributions; elastic scattering and vibrational transitions

Figure 5a displays the elastic angular distributions for COS at 1.0 eV in the $^2\Pi$ resonance region measured at two temperatures T. At room temperature, the present effective DCS agrees well with the results obtained by Sohn et al. at 1.15 eV [14].

Even at $T = 300$ K, as much as 17% of the COS molecules are in vibrationally excited states, which are considered to modify the elastic DCS σ_{00} for the ground vibrational state (000). For the purpose of extracting σ_{00} from the data taken at the two temperatures, we define an effective elastic DCS σ_{**} that accounts for the contributions from all the excited vibrational states. It depends on T, in principle, unless the elastic DCS is the same for all excited states with an appreciable population. However, we assume it to be independent of T for simplicity, and use equation (2) retaining only two terms. One might have some reservations about the significance of the quantity σ_{**}, but it should certainly help obtain a more reliable σ_{00} than the measured elastic cross section itself.

The lower figure of Figure 5a shows σ_{00} thus extracted. It clearly shows a sharp minimum, whereas σ_{**}, representing mainly the effects of bending excitation (judging from the populations found in Tab. 2), is much smaller

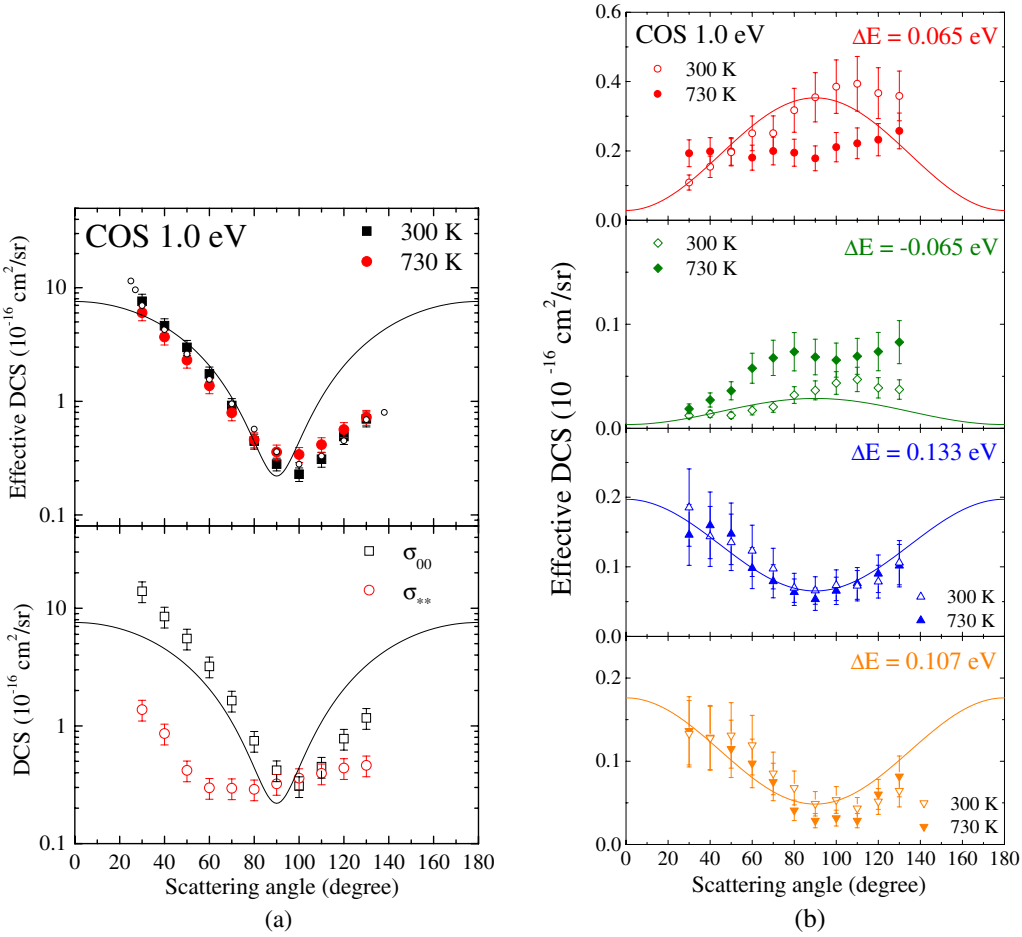

Fig. 5. Angular distributions for electron scattering by COS for $E = 1.0$ eV and $T = 300$ and 730 K (present results). Solid curves: fitting using the Read model [67]; see text. (a) Elastic scattering. Upper figure: measured data. ○: Sohn et al. [14] for 1.15 eV at room temperature. Lower figure: extracted elastic cross section for the ground vibrational state (σ_{00}) and the effective elastic cross section for all excited vibrational states (σ_{**}); see text. (b) Vibrational excitation and superelastic scattering. $\Delta E = 0.065$ eV: (000)–(010), (010)–(100)(020), etc. $\Delta E = -0.065$ eV: (010)–(000), (100)(020)–(010), etc. $\Delta E = 0.133$ eV: (000)–(020), (010)–(030), etc. $\Delta E = 0.107$ eV: (000)–(100), (010)–(110), etc.

and flatter. The angular distribution of σ_{00} exhibits the p-wave character (represented by the solid curve) stemming from the dominant partial wave in the π^* resonance orbital, though modified by the background rising toward the forward direction mainly because of the dipolar charge distribution of COS.

The theoretical elastic DCS at 1.15 eV calculated in the fixed-nuclei (FN) approximation shows a much shallower minimum [18,20] than the present σ_{00} and than the effective DCS at room temperature including that by Sohn et al. [14]. This may be due partly to the insufficient accuracy of the interactions taken into account in the calculations, but also to the FN approximation.

In the impulse or adiabatic-nuclei approximation, which is valid in the present case except for extremely forward elastic scattering, the DCS for a vibrational transition $v_0 \to v$ is expressible as $\sigma_{v_0,v} = |\langle v_0(\mathbf{R})|f(\mathbf{R})|v(\mathbf{R})\rangle|^2$ in terms of the scattering amplitude $f(\mathbf{R})$ calculated at fixed nuclear positions collectively denoted by $\mathbf{R}$ and the vibrational wave functions $|v_0\rangle$ and $|v\rangle$, if the wave number of the incident electron is assumed to be only slightly changed by vibrational excitation or deexcitation. Then, we have the ground-state elastic DCS $\sigma_{00} = |\langle 0|f|0\rangle|^2$ and the vibrationally summed DCS $\sigma_{\rm sum} = \sum_v \sigma_{0v} = \sum_v \langle 0|f|v\rangle\langle v|f^*|0\rangle = \langle 0||f|^2|0\rangle$. Naturally, these two differ from each other, in general, the latter being the former plus the inelastic cross sections. In the FN formulation, however, the ground-state probability density is approximated by the delta function, and it follows that $\sigma_{\rm sum} = \sigma_{00}$. In other words, the cross section calculated in the FN approximation may be interpreted either as an approximation for the ground-state elastic DCS or as that for the vibrationally summed DCS. This should cause little problem if the elastic DCS dominates the summed DCS. When the elastic DCS is small just as is found at the minimum in the angular distribution of Figure 5a, however, the FN DCS may be unreliable. Note that the energy-loss spectrum at 90° at 300 K in Figure 1 clearly proves the dominance of vibrational excitation over elastic scattering.

Incidentally, elastic scattering of a charged particle by a polar molecule in the FN or adiabatic nuclear rotation approximation is known theoretically to lead to a divergent ICS because of the divergence in the DCS for forward scattering due to the dipole interaction. In reference [18] this divergence is artificially avoided by truncating the correct infinite sum over the partial wave at some arbitrary finite number of terms, the numerical result depending on this arbitrary choice of the cutoff. In reference [17] the long-range dipole potential is totally neglected, resulting in no divergence problems at the cost of the accuracy in the forward DCS, and hence, in the ICS. Bettega et al. [19] and Gianturco and Stoecklin [20] take proper account of the infinite number of partial waves by applying the dipole-Born closure procedure, leading to a finite ICS.

For determining ICS from the DCS measured in the crossed-beam experiment, extrapolation into forward and backward DCSs is inevitable. The dipole-Born approximation for purely rotational transitions averaged over the T-dependent initial rotational distribution would be reasonable for this purpose as far as extremely forward scattering is concerned. For connection to the measured DCS at the smallest scattering angle, further theoretical improvement is needed.

Figure 5b shows angular distributions for vibrational excitation and deexcitation represented by four values of the energy loss ΔE, of which $\Delta E = 0.065$ eV refers to the mixture of σ_{01}, σ_{12}, etc., and $\Delta E = -0.065$ eV to the mixture of σ_{10}, σ_{21}, etc., the mixture ratios depending on T according to the thermal distribution. The present energy resolution is insufficient for resolving the energy-loss peaks for the other two values of ΔE, corresponding to near-degenerate vibrational states in group 2 of Table 2. However, a line-shape analysis was applied to separate σ_{02} (with some contributions from σ_{13} mixed in) into excitation to (100) (with some mixture of the transition (010)→(110)) and to (020) (with some (010)→(030)).

Significant T dependence is evident for $\Delta E = 0.065$ eV, but less so for the higher excitation. A conspicuous increase with the temperature is found in the superelastic effective DCS for $\Delta E = -0.065$ eV. This must be due mainly to the great change in the excited-state population $1 - P_0(T)$ with T, as is discussed in Section 3.1; the value of $1 - P_0(T)$ for COS increases by a factor of 3.7 from 17% at 300 K to 63% at 730 K. Any deviation of the temperature effect from the ratio 3.7 is due to the difference between σ_{10} and the DCS for deexcitation from the vibrational levels higher than (010). This difference is also the origin of the observed different shapes of the angular distributions at different T; the population of the levels higher than (010) is 0.23 times $P_1(T)$ at 300 K, but is 1.4 times $P_1(T)$ at 730 K.

Experimental resonance angular distributions are often compared with the prediction of a simple version of Read's model [66,67]. For a molecule belonging to the point group $C_{\infty v}$ the DCS for vibrational transitions via a $^2\Pi$ resonance in such a model would behave as $\sim(1 + 7\cos^2\theta)$ for $\sigma \rightarrow \Pi \rightarrow \sigma$ transitions and $\sim(2 - \cos^2\theta)$ for $\sigma \rightarrow \Pi \rightarrow \pi$ and $\pi \rightarrow \Pi \rightarrow \sigma$ transitions (referred to as the Read model in the following), where π is for a vibrational state excited by an odd number of bending quanta (groups 1 and 3, for example) and σ for any other vibrational state (groups 0 and 2, for example) [15]. The lower two figures in Figure 5b correspond to mixtures of the $\sigma \rightarrow \Pi \rightarrow \sigma$ transitions σ_{02} and σ_{13}, and the Read model (solid curve) reproduces the DCS fairly well for both temperatures T.

On the other hand, the upper two figures, corresponding to the $\sigma \rightarrow \Pi \rightarrow \pi$ and $\pi \rightarrow \Pi \rightarrow \sigma$ transitions, indicate the inapplicability of this simple model. This model should be applied, in principle, to state-to-state cross sections. Unfortunately, the statistical uncertainty in the measured effective cross sections actually prohibits reliable extraction of the state-to-state cross sections. It should be noted, however, that the measured T-dependent effective DCSs in the top two figures in Figure 5b would show the shape $\sim(2 - \cos^2\theta)$ if both σ_{01} and σ_{12} (and hence, σ_{10} and σ_{21} according to the principle of detailed balance) satisfied this shape. Judging from the fact that the data taken at 300 K look nearly like $\sim(2 - \cos^2\theta)$, the possibility would be that σ_{01} has a shape resembling $\sim(2 - \cos^2\theta)$ and that σ_{12} has quite a different shape because of the significant shift from the point group $C_{\infty v}$ upon bending.

Resonance angular distributions are also displayed for CO_2 at $E = 3.5$ eV in Figure 6 in a way similar to Figure 5 for COS. The elastic scattering data in Figure 6a reveals that the temperature effect is not quite significant in comparison to the statistical uncertainty. The ground-state DCS σ_{00} is extracted from the data at two temperatures $T = 310$ and 720 K by using an effective excited-state DCS σ_{**}, just as for the case of COS.

The result is consistent with previously reported elastic DCS in the $^2\Pi_u$ resonance region [44,68]. It shows a typical shape of a p-wave resonance with a considerable amount of in-phase f-wave mixed in for the valley around 90° to be quite broad in comparison with the case of COS, where a sharp dip of nearly pure p-wave shape is observed. The excited DCS σ_{**} is larger than σ_{00} by 10 to 40% up to a scattering angle of 100°, but then gets smaller than σ_{00} beyond this angle. The elastic DCS σ_{11} for the bending-excited state (010) at $E = 3.8$ eV, extracted by Johnstone et al. [69] from the data measured between $T = 35$ °C and 220 °C, is more than double σ_{00} and decreases monotonically from 20 to 80°. Incidentally, the population of the state (010) is 91% of all excited states at $T = 310$ K and 57% at 720 K. This may be of help in qualitative understanding of the significant difference between the reported σ_{11} and our σ_{**}.

The vibrational excitation and superelastic DCSs are found in Figure 6b. The unresolved second energy-loss peak on the right side of the elastic peak in the energy-loss spectrum is shape-analyzed and separated into two components corresponding, mainly, to excitation from (000) to the two members (FRI, FRII) of the lowest Fermi dyad. The results from Antoni et al. [56], measured for $E = 3.8$ eV and at room temperature, are also included.

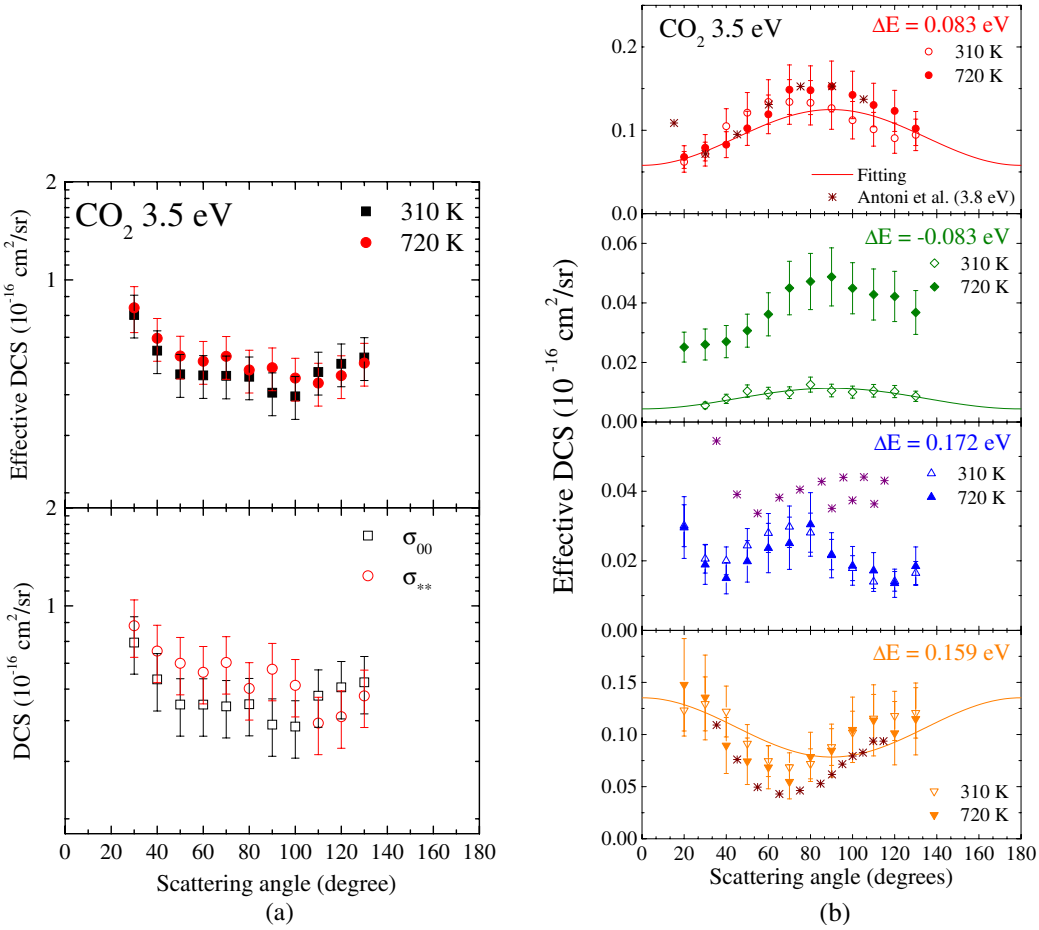

Fig. 6. Angular distributions for electron scattering by CO_2 for $E = 3.5$ eV and $T = 310$ and 720 K. (a) Elastic scattering. Upper figure: measured data. Lower figure: extracted elastic cross section for the ground vibrational state (σ_{00}) and the effective elastic cross section for all excited vibrational states (σ_{**}); see text. (b) Vibrational excitation and superelastic scattering. Solid curves: fitting due to the Read model [67]; see text. $*$: Antoni et al. [56] measured at $E = 3.8$ eV at room temperature. $\Delta E = 0.083$ eV: (000)–(010), (010)–(100)(020), etc. $\Delta E = -0.083$ eV: (010)–(000), (100)(020)–(010), etc. $\Delta E = 0.172$ eV: (000)–(FRII), etc. $\Delta E = 0.159$ eV: (000)–(FRI), etc. FRI, FRII: group 2 Fermi dyad.

Contrary to the situation in Figure 5b for COS, the Read model looks relatively reasonable for the transitions $\sigma \rightarrow \Pi \rightarrow \pi$ and $\pi \rightarrow \Pi \rightarrow \sigma$ between $\theta = 30°$ and 130° but not for $\sigma \rightarrow \Pi \rightarrow \sigma$, as has been found by Antoni et al. [56]. Thus, the predictability of the simple Read model is hard to tell in advance of the actual measurements.

The CO_2 molecule is the first example of the application of the resonance angular distribution model by Andrick and Read [67]. They retained three partial waves in each of the incident and scattered electron waves, and their amplitudes and phases have been determined by a least-squares fit to the measured DCS for excitation to (010) and to FRII (referred to as (100) in Ref. [67]). This procedure has been criticized by Antoni et al. [56] for too many fitting parameters and for some other reasons including the objection to the dominance of the f wave in the excitation of FRII.

The superelastic DCS at 720 K is much larger and has a somewhat different shape than that at 310 K. This is similar to the case of the superelastic DCS for COS, found in Figure 5b. As is already explained for COS, this must be due to a significant change in the population distribution, together with the dependence of the DCS on the initial vibrational state. The excited-state population $1 - P_0(T)$ for CO_2 increases by a factor of 5.3 from 9% at 310 K to 48% at 720 K. Furthermore, the population of the levels higher than (010) is 0.10 times $P_1(T)$ at 310 K, but is 0.75 times $P_1(T)$ at 720 K.

4 Summary

Absolute excitation functions for electron-impact vibrational excitation/deexcitation of the COS molecule and for vibrationally elastic scattering were measured for gas temperatures T of 300, 530, and 730 K, for electron energies E from 0.5 to 3.0 eV, and mainly at a scattering angle θ of 90°. The T dependence is clearly visible. Using the known vibrational population distributions in thermal equilibrium and the principle of detailed balance, these measured excitation functions were decomposed into the contributions from state-to-state vibrational transition

cross sections involving up to the second bending overtone (030) in the ground electronic state. Previously reported excitation functions for the CO_2 molecule [10] were also remeasured for 300, 520, and 830 K, for E from 1.5 to 6.0 eV, and at $\theta = 90°$, and were decomposed into state-to-state cross sections.

Both the profile of the $^2\Pi$ resonance for COS at ∼1.2 eV and that of the $^2\Pi_u$ resonance for CO_2 at ∼3.8 eV, both at $\theta = 90°$, are shifted to lower energies as the initial vibrational state is excited, i.e., as the molecule bends, roughly speaking. Similar lowering was also observed previously for the $^2\Pi$ resonance for N_2O at ∼2.3 eV [11]. The width at half maximum of the resonance structure changes with the initial vibrational state only slightly for the impulse-limit $^2\Pi$ resonances in COS and N_2O [11], whereas the overall boomerang envelope for CO_2 becomes narrower and narrower as the initial state is excited. The knowledge of the complex potential energy surface of an impulse-limit resonance would directly give an idea of the resonance behavior as the initial state changes. On the other hand, the multidimensional nuclear dynamics on the complex potential or coupled complex potentials has to be studied in detail for elucidating a boomerang resonance in a polyatomic molecule. As the molecule bends, the magnitude of the maximum cross section increases for COS and N_2O [11], whereas it decreases for CO_2.

The T dependence of the angular distribution of the electrons resonantly scattered elastically or after exciting/deexciting COS at $E = 1.0$ eV and CO_2 at 3.5 eV was measured at room temperature and at a higher T. The temperature effect is evident in most cases. Some of the differential cross sections are found to have a shape resembling a linear function of $\cos^2\theta$, either concave upward or downward versus θ depending on the symmetry of the vibrational wave functions, which follows from a simple model due to Andrick and Read [67]. However, others exhibit quite a different shape, suggesting the need of more terms in the partial-wave expansion in their model.

Since the 1980s, Prof. M. Allan, has been the driving force behind the use of high resolution low-energy electron spectroscopy for clarifying resonance features in atoms and molecules. Over the years, we have learned very much from his achievements and it is a pleasure, therefore, to contribute within this topical issue in his honor with our current results of changes of the resonance parameters in a linear molecule as it bends. This work was conducted under the support of the Japanese Ministry of Education, Culture, Sport, Science and Technology. HK was supported by Grant-in-Aid for JSPS, Grant Number 205032. PLV acknowledges the Portuguese National Funding Agency FCT through research grants PTDC/FIS-ATO/1832/2012 and UID/FIS/00068/2013. PLV also acknowledges his Visiting Professor position at Sophia University, Tokyo, Japan.

Author contribution statement

M.H., Y.I., H.K., P.L.V., H.T., and I.S. contributed to the experiment, data analysis and discussion parts. D.M., Y.T. and K.F. at Kato Denka Kogyo Co., Ltd. supplied the COS gas sample and suggested the experimental gas handling system.

References

1. M. Halka, P.G. Harris, A.H. Mohagheghi, R.A. Reeder, C.Y. Tang, H.C. Bryant, J.B. Donahue, C.R. Quick, Phys. Rev. A **48**, 419 (1993)
2. J.R. Harries, J.P. Sullivan, J.B. Sternberg, S. Obara, T. Suzuki, P. Hammond, J. Bozek, N. Berrah, M. Halka, Y. Azuma, Phys. Rev. Lett. **90**, 133002 (2003)
3. S. Kar, Y.K. Ho, J. Phys. B **43**, 135003 (2010)
4. C. Chin, R. Grimm, P. Julienne, E. Tiesinga, Rev. Mod. Phys. **82**, 1225 (2010)
5. Y. Wang, J.P. D'Incao, B.D. Esry, Adv. At. Mol. Opt. Phys. **62**, 1 (2013)
6. T.N. Rescigno, W.A. Issacs, A.E. Orel, H.D. Meyer, C.W. McCurdy, Phys. Rev. A **65**, 032716 (2002)
7. C.W. McCurdy, W.A. Isaacs, H.-D. Meyer, T.N. Rescigno, Phys. Rev. A **67**, 042708 (2003)
8. R. Renner, Z. Phys. **92**, 172 (1934)
9. D.G. Hopper, A.C. Wahl, R.L.C. Wu, T.O. Tiernan, J. Chem. Phys. **65**, 5474 (1976)
10. H. Kato, H. Kawahara, M. Hoshino, H. Tanaka, L. Campbell, M.J. Brunger, Chem. Phys. Lett. **465**, 31 (2008)
11. H. Kato, M. Ohkawa, H. Tanaka, I. Shimamura, M.J. Brunger, J. Phys. B **44**, 195208 (2011)
12. C. Szmytkowski, M. Zubek, Chem. Phys. Lett. **57**, 105 (1978)
13. M. Tronc, R. Azria, in *Symposium on Electron-Molecule Collisions, Invited Papers*, edited by I. Shimamura, M. Matsuzawa (University of Tokyo Press, Tokyo, 1979), p. 105
14. W. Sohn, K.H. Kochem, K.M. Scheurlein, K. Jung, H. Ehrhardt, J. Phys. B **20**, 3217 (1987)
15. R. Abouaf, J. Pommier, S. Cvejanovic, B. Saubamea, Chem. Phys. **188**, 339 (1994)
16. T.H. Hoffmann, H. Hotop, M. Allan, J. Phys. B **41**, 195202 (2008)
17. M.G. Lynch, D. Dill, J. Siegel, J.L. Dehmer, J. Chem. Phys. **71**, 4249 (1979)
18. S.E. Michelin, T. Kroin, I. Iga, M.G.P. Homem, H.S. Miglio, M.T. Lee, J. Phys. B **33**, 3293 (2000)
19. M.H.F. Bettega, M.A.P. Lima, L.G. Ferreira, Phys. Rev. A **70**, 062711 (2004)
20. F.A. Gianturco, T. Stoecklin, Chem. Phys. **332**, 145 (2007)
21. M.H.F. Bettega, M.A.P. Lima, L.G. Ferreira, Phys. Rev. A **72**, 014702 (2005)
22. H. Murai, Y. Ishijima, T. Mitsumura, Y. Sakamoto, H. Kato, M. Hoshino, F. Blanco, G. Garcia, P. Limao-Vieira, M.J. Brunger, S.J. Buckman, H. Tanaka, J. Chem. Phys. **138**, 054302 (2013)
23. G.P. Karwasz, R.S. Brusa, A. Zecca, Riv. Nuovo Cimento **24**, 1 (2001)
24. *CRC Handbook of Chemistry and Physics*, edited by D.R. Lide, 88th edn. (CRC Press, Boca Raton, Florida, 2007-2008)
25. K. Tanaka, H. Ito, K. Harada, T. Tanaka, J. Chem. Phys. **80**, 5893 (1984)
26. G. Maroulis, M. Menadakis, Chem. Phys. Lett. **494**, 144 (2010)

27. G. Herzberg, *Molecular Spectra and Molecular Structure, Infrared and Raman Spectra of Polyatomic Molecules* (van Nostrand, New York, 1945), Vol. 2
28. J.E. Johnson, T.S. Bates, J. Geophys. Res.: Atmos. **98**, 23443 (1993)
29. M. Pham, J.-F. Mueller, G.P. Brasseur, C. Granier, G. Megie, J. Geophys. Res.: Atmos. **100**, 26061 (1995)
30. M. Chin, D.D. Davis, J. Geophys. Res.: Atmos. **100**, 8993 (1995)
31. D.C. Thornton, A.R. Bandy, B.W. Blomquist, B.E. Anderson, J. Geophys. Res.: Atmos. **101**, 1873 (1996)
32. E. Kjellstrom, J. Atmos. Chem. **29**, 151 (1998)
33. B. Bezard, C. De Bergh, D. Crisp, J.P. Maillard, Nature **345**, 508 (1990)
34. E. Lellouch, et al., Nature **373**, 592 (1995)
35. M.E. Palumbo, A.G.G.M. Tielens, A.T. Tokunaga, Astrophys. J. **449**, 674 (1996)
36. M.E. Palumbo, T.R. Geballe, A.G.G.M. Tielens, Astrophys. J. **479**, 839 (1997)
37. Kanto Denki Kogyo Co., LTD. (private communication)
38. L.G. Christophorou, J. Olthoff, Adv. At. Mol. Opt. Phys. **44**, 156 (2001)
39. T. Tanaka, C. Makochekanwa, H. Tanaka, M. Kitajima, M. Hoshino, Y. Tamenori, E. Kukk, X.J. Liu, G. Pruemper, K. Ueda, Phys. Rev. Lett. **95**, 203002 (2005)
40. T. Tanaka, M. Hoshino, R.R. Lucchese, Y. Tamenori, H. Kato, H. Tanaka, K. Ueda, New J. Phys. **12**, 123017 (2010)
41. T. Tanaka, M. Hoshino, H. Kato, J.R. Harries, Y. Tamenori, K. Ueda, H. Tanaka, J. Electron Spectrosc. Relat. Phenom. **164**, 24 (2008)
42. M. Hoshino, T. Odagiri, M. Kitajima, K. Shigemura, N. Watanabe, J. Adachi, H. Tanaka, J. Electron Spectrosc. Relat. Phenom., in preparation.
43. H. Tanaka, L. Boesten, D. Matsunaga, T. Kudo, J. Phys. B **21**, 1255 (1988)
44. H. Tanaka, T. Ishikawa, T. Masai, T. Sagara, L. Boesten, M. Takekawa, Y. Itikawa and M. Kimura, Phys. Rev. A **57**, 1798 (1998)
45. S.K. Srivatava, A. Chutjian, S. Trajmar, J. Chem. Phys. **63**, 2659 (1975)
46. L. Boesten, H. Tanaka, At. Data Nucl. Data Tables **52**, 25 (1992)
47. J.N.H. Brunt, G.C. King, F.H. Read, J. Phys. B **10**, 1289 (1977)
48. R.E. Kennerly, Phys. Rev. A **21**, 1876 (1980)
49. A. Herzenberg, in *Electron-Molecule Collisions*, edited by I. Shimamura, K. Takayanagi (Plenum, New York, 1984), p. 191
50. A. Herzenberg, F. Mandl, Proc. Roy. Soc. A **270**, 48 (1962)
51. A. Herzenberg, J. Phys. B **1**, 548 (1968)
52. D.T. Birtwistle, A. Herzenberg, J. Phys. B **4**, 53 (1971)
53. M.J.W. Boness, G.J. Schuz, Phys. Rev. A **9**, 1969 (1974)
54. C. Szmytkowski, M. Zubek, J. Phys. B **10**, L31 (1977)
55. I. Čadež, F. Gresteau, M. Tronc, R.I. Hall, J. Phys. B **10**, 3821 (1977)
56. Th. Antoni, K. Jung, H. Ehrhardt, E.S. Chang, J. Phys. B **19**, 1377 (1986)
57. M. Allan, Phys. Rev. Lett. **87**, 033201 (2001)
58. L.D. Landau, E.M. Lifshitz, *Quantum Mechanics*, 3rd edn. (Pergamon, Oxford, 1977), Chap. 18
59. M. Allan, S.F. Wong, Phys. Rev. Lett. **41**, 1791 (1978)
60. J.N. Bardsley, J.M. Wadehra, Phys. Rev. Lett. **41**, 1795 (1978)
61. J.N. Bardsley, J.M. Wadehra, Phys. Rev. A **20**, 1398 (1979)
62. R.N. Compton, J.N. Bardsley, in *Electron-Molecule Collisions*, edited by I. Shimamura, K. Takayanagi (Plenum, New York, 1984), p. 275
63. S.I. Drozdov, Sov. Phys. J. Exp. Theor. Phys. **1**, 591 (1955)
64. S.I. Drozdov, Sov. Phys. J. Exp. Theor. Phys. **3**, 759 (1956)
65. J. Ferch, C. Masche, W. Raith, L. Wiemann, Phys. Rev. A **40**, 5407 (1989)
66. F.H. Read, J. Phys. B **1**, 893 (1968)
67. D. Andrick, F.H. Read, J. Phys. B **4**, 389 (1971)
68. J.C. Gibson, M.A. Green, K.W. Trantham, P.J.O. Teubner, M.J. Brunger, J. Phys. B **32**, 213 (1999)
69. W.M. Johnstone, M.J. Brunger, W.R. Newell, J. Phys. B **32**, 5779 (1999)